 CMES, vol.3, no.4, pp.497-506, 2002

A Numerical Model for Elastoplastic Rough Contact

P. Sainsot,[1] **C. Jacq,**[2] **and D. Nélias**[1]

Abstract: Pressure distributions calculated in the simulation of rough contacts show high values and induce high stresses just beneath the surface. These stresses often exceed the yield strength of the material, therefore, a purely elastic contact model is restrictive. Plastic flow occurs and modifies the surface shape and consequently modifies the surface pressure.

This paper presents a numerical model for 3D-elastoplastic rough contact. It allows the determination of real pressure and permanent surface displacement (flattening of asperities) as well as residual stresses and plastic strains useful in fatigue analysis. The material is assumed to follow the Von-Mises yield criterion with isotropic hardening.

The use of FFT in the numerical procedure allows a large number of meshing points so real surfaces obtained from a measurement can be considered.

keyword: Contact, plasticity, FFT, boundary integral

Nomenclature

h	initial local distance between two bodies
p	local pressure on the surface
s	deviatoric stress tensor
s^e	elastic deviatoric stress tensor
s^r	residual deviatoric stress tensor
u	displacement vector
u^e	elastic displacement vector
u^r	residual displacement vector
C_{klij}	influence functions of plastic strains upon stresses
D_{jki}	influence functions of plastic strains upon displacements
E	Young modulus
$[M]$	elasticity matrix
N_c	number of points on Γ_c
N_i	number of points of Γ_c inside the real contact area
N_e	number of points of Γ_c outside the real contact area
N_p	number of points in Ω_p
S_{kij}	influence functions of pressure upon stresses
U_{ji}	influence functions of pressure upon displacements
δ	local distance between two bodies
δ_{ij}	Kronecker symbol
ε^p	plastic strain tensor
ε	strain tensor
ε^e	elastic strain tensor
ε^r	residual strain tensor
ν	Poisson coefficient
σ	stress tensor
σ^e	elastic stress tensor
σ^r	residual stress tensor
σ_y	traction yield strength
Γ_c	potential contact surface
Ω_p	plastic zone
μ	Lamé coefficient
B, C, n	Swift law parameters

1 Introduction

The rough contact problem has been studied for many years because of its numerous implications in tribology: friction, wear, fatigue and damage. Recent review articles on contact mechanics [Barber and Ciavarella (2000)] and tribology [Tichy and Meyer (2000)] discuss many important phenomena of tribological contact and em-

[1] Laboratoire de Mécanique des Contacts (UMR CNRS 5514)
INSA Lyon
20 Av. A. Einstein
69621 Villeurbanne Cedex, France
[2] SNECMA, Direction Technique
Centre de Villaroche
77550 Moissy Cramayel, France

phasize the importance of understanding the effects of roughness and plasticity. Modeling these effects has taken two main paths.

The statistical approach to rough contact problems, investigated by Greenwood and Williamson (1966) and later by Archard, Hunt, and Onions (1975), yields important results concerning the behavior at the contact scale (contact area, normal approach). Simple plasticity ideas have recently been incorporated into this approach [Zhao, Maietta, and Chang (2000)]. However, statistical models cannot predict the distribution of contact spots, and local pressure or stress values, which play a major role in material fatigue and damage.

With the increase in computer performance, numerical models have been developed for the study of complex contact problems [Kalker (1990)]. Some of them deal with rough contact [Webster and Sayles (1986), Seabra and Berthe (1987), Bailey and Sayles (1991)]. When modeling rough contacts it is necessary to take into account the multi-scale nature of surface topography. The surface grid has to be as large as possible to account for the large wavelength of the roughness components but also as fine as possible to include the short wavelength of the roughness. Such grids lead to large numbers of nodes and equations to solve. This aspect is one of the most difficult points in the 3D contact modeling. Recently, fast methods have appeared for solving 3D rough contact problems, some of them are based on the multilevel technique [Lubrecht and Ioannides (1991)], other on Fast Fourier Transforms [Nogi and Kato (1997)].

Although these models assumed elastic material behavior, their results show that this assumption was often improper. The current FFT methods, which can address the contact of elastically coated surfaces [Polonsky and Keer (2000a)] or thermal distorsion, may also introduce plasticity as an asperity pressure limit, without considering plastic flow [see for example Liu, Wang, and Liu (2001)]. On the other hand, the use of the finite element method, which readily treats elastoplastic behavior, leads to costly calculations when both surface roughness and bulk behavior have to be taken into account [Komvopoulos and Choi (1992)].

In order to overcome these difficulties, a numerical method based on a boundary integral formulation for an elastoplastic half space is presented in this paper. This method is applied to 3D elastoplastic contact problems with Von-Mises yielding and isotropic hardening. This new numerical method, which is an extension of the method presented by Mayeur, Sainsot, and Flamand (1995), is presented in detail elsewhere [Jacq, Nélias, Lormand, and Girodin (2002)]. The main assumptions of the proposed analysis are that of small strains and rotations, and half infinite bodies. As only parts of the half plane (i.e. contact surface and plastic zone) have to be discretized, the numerical system is dramatically reduced. Also, the numerical system is well suited for an FFT-based scheme that is presented here to increase the speed of computation.

2 Contact Model

The contact problem consists of finding a pressure distribution p(**x**) between two surfaces. Denoting h(**x**) the initial gap between the surfaces before loading, the local gap between the deformed surfaces δ(**x**) after loading can be written as:

$$\delta(\mathbf{x}) = u(\mathbf{x}) + h(\mathbf{x}) \tag{1}$$

where u is the normal displacement difference. The main feature of the contact problem consists of the mixed boundary conditions that arise on the contact surface. Furthermore, these boundary conditions are explained with inequalities, and the contact surface is unknown. So, we have to define a potential contact surface, Γ_c, that contains the real contact surface. Γ_c is subjected to the boundary conditions:

$$\left.\begin{array}{l} \delta \geq 0 \\ p \geq 0 \end{array}\right\} \text{ on } \Gamma_c \tag{2}$$

The first condition is a non penetration condition, and the second implies that surface pressure are only positive (x_3 axis is defined entering in the body, see figure 1).

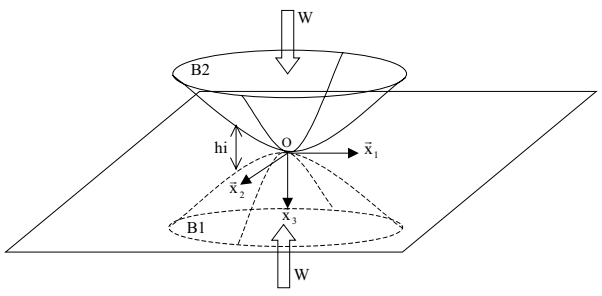

Figure 1 : Contact problem description.

Each body has to satisfy stress equilibrium (bulk equation) and is submitted to additional classical boundary conditions, i.e. displacements and/or forces prescribed on some parts of its surface. When the contact area is small compared to the dimensions of the body, and when surface slopes are small, the solids in contact can be considered as two half spaces.

For elastic bodies the Boussinesq relations between load and displacement at the surface can then be used [Johnson (1985)]. In addition, this assumption enables the substitution of the classical boundary conditions (displacements or forces prescribed) by a load or rigid body movement condition. The use of the Boussinesq load-displacement relation leads to:

$$u(\mathbf{x}) = \int_{\Gamma_c} U(\mathbf{x},\boldsymbol{\xi})\, p(\boldsymbol{\xi})\, d\Gamma(\boldsymbol{\xi}) \tag{3}$$

where $\mathbf{x}$ and $\boldsymbol{\xi}$ are two points on the surface, and $U(\mathbf{x},\boldsymbol{\xi})$ is the displacement at point $\mathbf{x}$ due to an unit load at point $\boldsymbol{\xi}$. This relation verifies stress equilibrium, elastic behavior and small strains assumption. As Γ_c is unknown, the procedure is iterative.

3 Elastoplastic Behavior

Elastoplastic material behavior is characterized by the appearance of strains, which are instantaneous, irrecoverable and are submitted to a threshold condition. The first characteristic means that plasticity is time independent, but the two others imply that it is a path dependent (dissipative) phenomenon.

Many different behaviors have been observed above the elastic limit, concerning materials and loading conditions. Thus many constitutive laws have been proposed to describe plasticity. Here we consider a material that obeys to the Von-Mises yield function and presents ***an isotropic*** hardening.

The yield condition is defined by:

$$f(\sigma_{ij},\varepsilon^p_{ij}) = \sqrt{\frac{3}{2} s_{kl} : s_{kl}} - B\left[C + \sqrt{\frac{3}{2}\varepsilon^p_{kl} : \varepsilon^p_{kl}}\right]^n = 0 \tag{4}$$

$$\text{with } s_{kl} = \sigma_{kl} - \frac{1}{3}\sigma ii\,\delta_{kl}$$

s_{kl} is the deviatoric stress tensor, ε^p_{ij} the plastic strain tensor components, B, C and n are the parameters of the Swift law $\sigma = B[C+\varepsilon^p]^n$ and δ_{kl} the Kronecker symbol. In a nine dimensional space (the deviatoric stress space), the elastic domain is represented by a sphere.

Plastic flow is governed by:

$$\dot{\varepsilon}^p_{ij} = \frac{3}{2}\frac{1}{nB}\left(\frac{B}{\sqrt{\frac{3}{2}s_{kl} : s_{kl}}}\right)^{1-\frac{1}{n}} \frac{3 s_{kl} : \dot{s}_{kl}}{\frac{3}{2} s_{kl} : s_{kl}} s_{ij} \tag{5}$$

$$\text{if } f(\sigma_{ij},\varepsilon^p_{ij}) = 0 \text{ and } df = 0$$

where the dot denotes the rate of the variables.

4 Boundary Integral Formulation

When the contact area is small compared to the dimensions of bodies, the extent of the plastic zone is small. As discussed before, finite element methods, which need a discretization of the entire bodies to represent bulk behavior, lead to costly calculations for modeling a rough contact. Keeping the half space assumption, often used in contact mechanics, a boundary integral formulation is used, which allows us to discretize only the zone where plasticity occurs (in addition to contact surface).

When a half space is subjected to a load distribution at its surface Γ, together with an inelastic strain distribution in its volume Ω, displacements at each point ξ can be expressed as follow:

$$u_i(\xi) = \int_\Gamma u^*_{ij}(\xi,x)\; p_j(x)\; d\Gamma(x) + \int_\Omega \left[\sigma^*_{jki}(\xi,x) - \nu\, \sigma^*_{lli}(\xi,x)\right]\; \varepsilon^p_{jk}(x)\; d\Omega(x) \tag{6}$$

where $u^*_{ij}(\xi,x)$ and $\sigma^*_{jki}(\xi,x)$ correspond respectively to components (j) and (jk) of displacement and strain at point x due to a unit force applied in direction (i) at point ξ in a half plane.

This expression has been proposed by Telles and Brebbia (1981), and is derived from the application of the reciprocal theorem with initial strains, using the fundamental solution of a half space domain with a free boundary; using this formulation, a distinct class of boundary element methods has been successfully used in soil mechanics problems [Telles and Brebbia (1981), Brebbia, Telles, and Wrobel (1984)].

The application of a boundary integral formulation implicitly accounts for the elastic (linear) part of the ma-

terial behavior in bulk. The use of the half space fundamental solution implicitly accounts for the geometry. Thus, only the discretization of the loading surface Γ_c and the plastic zone Ω_p is necessary.

As discussed before, the elastoplastic stress tensor σ is divided into an elastic part σ^e and a residual part σ^r:

$$\sigma = \sigma^e + \sigma^r$$

The corresponding strains are:

$$\varepsilon = \varepsilon^e + \varepsilon^r \tag{7}$$

They are related to the stresses by:

$$\varepsilon = [M]\sigma \tag{8}$$
$$\varepsilon^e = [M]\sigma^e \tag{9}$$
$$\varepsilon^r = [M]\sigma^r + \varepsilon^p \tag{10}$$

where $[M]$ is the compliance matrix.

Following the same procedure, displacements can be expressed as:

$$u = u^e + u^r \tag{11}$$

where u^e and u^r are defined by:

$$u_i^e(\xi) = \int_\Gamma u_{ij}^*(\xi,x)\ p_j(x)\ d\Gamma(x) \tag{12}$$

$$u_i^r(\xi) = \int_\Omega \left[\sigma_{jki}^*(\xi,x) - \nu\sigma_{lli}^*(\xi,x)\right]\ \varepsilon_{jk}^p(x)\ d\Omega(x) \tag{13}$$

Each of these two parts has a physical meaning: u^e corresponds to the solution for a purely elastic material, and u^r corresponds to the stabilized state when the half space is unloaded, since no plasticity occurs during unloading because of the chosen plasticity model.

From a mathematical point of view, u^e is the solution of the associated homogeneous problem of elasticity with initial strains which satisfy the boundary conditions, and u^r is a specific solution of the total problem which does not modify the boundary conditions.

5 Resolution/Numerical Procedure

5.1 Discretization

Following Seabra and Berthe (1987), the potential contact surface Γ_c is discretized into N_c elements of the same size where the pressure is assumed to be constant. N_i and N_e are the numbers of elements of Γ_c inside and outside the real contact area ($N_i + N_e = N_c$). Furthermore, the plasticized volume is discretized into N_p rectangular cells where plastic strains are assumed to be constant. Equation (6) can be rewritten as:

$$u_i(\xi) = \sum_{n=1}^{N_i}\left\{\int_{\Gamma_n} u_{ij}^* d\Gamma\right\} p_j(n) + \sum_{m=1}^{N_p}\left\{\int_{\Omega_m}\left[\sigma_{jki}^* - \nu\sigma_{lli}^*\right] d\Omega\right\}\varepsilon_{jk}^p(m) \tag{14}$$

where Γ_n and Ω_m are the local domains associated to elements n and m.

Integrals over each element are calculated analytically, as allowed by the simple interpolation (constant). Therefore, equation (14) results in:

$$u_i(\xi) = \sum_{n=1}^{N_i} U_{ji}(n,\xi)\ p_j(n) + \sum_{m=1}^{N_p} D_{jki}(m,\xi)\ \varepsilon_{jk}^p(m) \tag{15}$$

U_{ij} and D_{ijk} are analytical functions for the point ξ. They can be derived and combined to give the stress components in the form:

$$\sigma_{ij}(\xi) = \sum_{n=1}^{N_i} S_{kij}(n,\xi)\ p_k(n) + \sum_{m=1}^{N_p} C_{klij}(m,\xi)\ \varepsilon_{jk}^p(m) \tag{16}$$

Expressions of U_{ij} and S_{ijk} correspond to displacements and stresses due to a rectangular distribution of pressure on the half plane surface and can be found in Johnson (1985). Expressions of D_{ijk} and C_{ijkl} are the displacements and stresses due to an uniform distribution of plastic strains in a parallelepiped cell surrounded by an elastic half space. Displacement functions are given elsewhere [Jacq, Nélias, Lormand, and Girodin (2002)] and stress functions can be found from Chiu (1977, 1978). The use of a constant discretization step leads to a reduced number of stored coefficients.

Relations (1), (2) and (6) are then discretized, and the following two systems of equations are given:

Elastic system

$$u_i^e(n)=\sum_{m=1}^{N_i} U_{ji}(m,n)\,p_j(m) \quad n=1,N_c \tag{17}$$

$$u^e(n)+u^r(n)+h(n)=0 \quad n=1,N_i \tag{18}$$

$$p(n)>0 \quad n=1,N_i \tag{19}$$

$$u^e(n)+u^r(n)+h(n)>0 \quad n=N_i+1,N_i+N_e=N_c \tag{20}$$

$$p(n)=0 \quad n=N_i+1,N_i+N_e=N_c \tag{21}$$

When the pressure distribution on Γ_c is known, elastic stresses in bulk can be obtained using:

$$\sigma_{ij}^e(\xi)=\sum_{n=1}^{N_i} S_{kij}(n,\xi)\; p_k(n) \tag{22}$$

Residual system

$$\sigma_{ij}^r(n)=\sum_{m=1}^{N_p} C_{klij}(m,n)\;\varepsilon_{kl}^p(m) \quad n=1,N_p \tag{23}$$

$$\dot{\varepsilon}_{ij}^p=\frac{3}{2C\sigma_y^2}\left[\left(s_{ij}-C\varepsilon_{ij}^p\right)\dot{s}_{ij}\right]\left(s_{ij}-C\varepsilon_{ij}^p\right) \tag{24}$$

$$\text{if } f(n)=0 \text{ and } df(n)=0 \quad n=1,Np$$

Once the εP values are known, displacements on the surface can be obtained using:

$$u_i^r(n)=\sum_{m=1}^{N_p} D_{kli}(m,n)\;\varepsilon_{kl}^p(m) \qquad n=1,N_c \tag{25}$$

Only normal displacements will be computed. Tangential displacements are neglected.

5.2 Resolution

Elastic problem

For a given distribution of u^r, the elastic problem corresponds to an elastic contact problem with an apparent distance u^r + h instead of h. It has been solved using the multigrid method proposed by Lubrecht and Ioannides (1991). Elastic stresses are then computed using equation (22).

Residual problem

The residual problem required a step by step loading, to take the loading path into account. For a given load, a load increment is applied. From this load increment, a stress field increment $\dot{\sigma}^e$ can be calculated. Plastic strain increment is obtained using (24). Residual stress increment can then be determined from equation (23) and implemented in the plastic strain increment calculation. This process is repeated until convergence. Under relaxation must be used to reduce the number of iterations. Convergence difficulties can arise when hardening is low, i.e. when moderate or high plastic deformations are locally found (typically for the Swift law used when ε^p exceeds 5%), which however is beyond the domain of validity of the model (small strain assumption).

Once the solution is obtained for ε^p and σ^r, the displacements u^r are calculated using (25).

5.3 Coupling of the two parts

The two parts u^e and u^r are dependent. Each is the solution of a problem where the other is assumed to be known. Since the assumption of small strains and rotations is made, the elastic and the plastic solutions can be superposed. Thus another iterative process is used. Initially, we suppose that no plasticity occurs and elastic contact is solved with the conditions:

$$\begin{cases} h+u^e \geq 0 \\ \sigma^e \cdot n \geq 0 \end{cases}$$

The resulting stresses σ^e are used to determine the corresponding ε^p, σ^r, and u^r. Then $u^r$is used to solve another contact problem and this procedure is repeated until convergence. Under relaxation of u^r is used to improve convergence.

5.4 Validation

The methodology presented above has been computed in Fortran 90 under a Windows NT environment. More details on the theory and on the numerical procedure can be found in a previous paper mostly focused on the formulation of the elasto-plastic contact problem [Jacq, Nélias, Lormand, and Girodin (2002)]. An example of validation given previously is recalled here to attest the validity of the model.

A comparison with the commercial finite element code ABAQUS has been made. The validation test consist of the nano-indentation of a steel half space whose elastic

characteristics are E=210 Gpa and ν=0.3 for the Young modulus and Poisson coefficient. Its plastic behavior is described by the Swift's law whose parameter are B=1240 MPa , C=30 and n=0.085. The punch is a rigid sphere of 105μm radius. The evolution of the load with the rigid body displacement is plotted in figure 2. The results supplied by the FE code and by the SAC are identical. The formed print has a depth of about 80 nm. Because of the hardening model that has been chosen, no plasticity occurs during unloading. Therefore, the comparison of the unloading of the elastic indentation and the unloading of the elastic plastic indentation shows the influence of the geometry change. If the geometry would not change, the pressure would be the same in both cases, and the two unloading curves should be only shifted.

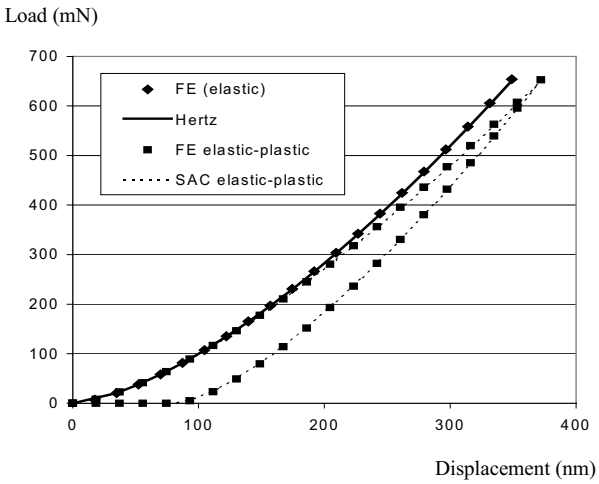

Figure 2 : Validation of the computer code from [Jacq, Nélias, Lormand, and Girodin (2002)]: Load vs rigid body displacement. Rigid punch and elastic-plastic half space.

6 Discrete Convolution Product Acceleration Method

The elastoplastic contact resolution is time consuming. This is primarily due to the calculation of convolution product of equations (22), (23) and (25). In order to improve the computational speed of the contact code, FFT are used to accelerate the calculation of convolution product.

Fourier transform has the property to change a convolution product in the spatial domain into term product in the frequency domain. However, when using discrete Fourier transform, the problem becomes periodic. Special care must then be taken to cancel this effect. Simply enlarging the computational domain for the periodic problem causes too great of a computational burden [Polonsky and Keer (2000b)]. Misunderstanding the difference between discrete convolution and continuous convolution also causes problems [Liu, Wang, and Liu (2000)].

Consider a pressure distribution given on N points. To calculate stresses in the bulk under the pressure distribution, 2N influence coefficients are required. If FFT is used to perform the convolution product, the period of the functions must be chosen following the relationship given by Brigham (1974) 2N+N-1, so that no overlap occurs. The convolution will be correct over the 3N-1 points and stresses over the N points. However, the zone where accurate stress is required is often narrow. It is then possible to reduce the period of the functions, depending upon the area of interest.

Consider a pressure distribution given on P points numbered from 0 to P-1. Accurate stresses are needed on points from ni to ne. The number of influence coefficients required for this calculation is given in equation (26).

$$Q = \max(\mathrm{ne}+1, P-\mathrm{ni}) \tag{26}$$

Consider a period of 2Q. The pressure is padded with zeros between P-1 and 2Q-1 points.

The convolution product can be written as

$$\sigma^e_{ij}(n) = \sum_{i=0}^{2Q-1} p_{k=3}(i) S_{ijk=3}(n-i) \tag{27}$$

Since the pressure is padded with zeros, equation (27) can be simplified

$$\sigma^e_{ij}(n) = \sum_{i=0}^{P-1} p_{k=3}(i) S_{ijk=3}(n-i) \tag{28}$$

The non overlapping condition is given by equation (29)

$$-Q+1 < n-i < Q-1 \tag{29}$$

From equation (28), one can write that

$$n - P + 1 \leq n - i \leq n \tag{30}$$

The interest area extend from ni to ne. Therefore equation (30) becomes

$$\text{ni} - P + 1 \leq n - i \leq \text{ne} \tag{31}$$

The definition of Q leads to

$$P - \text{ni} \leq Q; \text{ne} + 1 \leq Q; \text{ So } 1 - Q \leq n - i \leq Q - 1 \tag{32}$$

Equation (32) being equivalent to equation (29) the non overlapping condition is respected for the points located between ni and ne. The number of points required to prevent overlapping due to the use of FFT can then be reduced by considering the area where accurate stresses are required. Consider the following example described in figure 3. The pressure distribution is given on P=10 points. The stress field is required between point 2 and point 5. The number of influence coefficients required for calculation is 8=max(5+1,10-2). Therefore, pressure profile must be extended with zeros to point 15 before transforming.

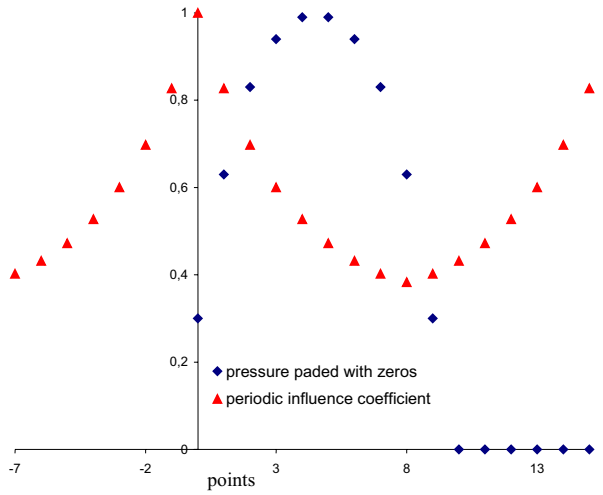

Figure 3 : Use of FFT and zero padding.

This method has been extended to two dimensional problems with no major difficulties, by making the same considerations on both directions independently. This process has also been applied to residual stress calculation and to residual displacement calculation. When calculating residual stresses or residual displacement, each depth has to be taken separately, since there is no convolution product along the vertical axis.

In order to still reduce the computational cost, several variables are joined before transforming. Consider the convolution product of equation (25). To compute this, it is necessary to transform plastic strain and influence coefficient, to make the term to term product in the frequency domain and then to make the inverse transform of the result, needing the computation of two FFT, one IFFT and a product for each of the six different strain components. Twelve FFT and six IFFT are then required to calculate residual displacement induced by each depth. Consider the complex influence coefficient and the complex plastic strain, constructed as shown in equation (33).

$$\begin{aligned} \overline{D}_{ikl} &= D_{ikl} + iD_{ik+1l} \\ \overline{\varepsilon}^p_{kl} &= \varepsilon^p_{kl} - i\varepsilon^p_{k+1l} \end{aligned} \tag{33}$$

Fourier transform of these complex strain and influence coefficient can be expressed as a function of the original Fourier transform of strain and influence coefficients (34).

$$\begin{aligned} \tilde{\overline{D}}_{ikl} &= \tilde{D}_{ikl} + i\tilde{D}_{ik+1l} \\ \tilde{\overline{\varepsilon}}^p_{kl} &= \tilde{\varepsilon}^p_{kl} - i\tilde{\varepsilon}^p_{k+1l} \end{aligned} \tag{34}$$

The term to term product can be made in the frequency domain (35). If the inverse Fourier transform is applied to this expression (36), the real part is the sum of two convolution products, and represents the contribution of ε^p_{kl} andε^p_{k+1l} to residual displacement. Hence, using this method, only six FFT and three IFFT are required to calculate residual displacement, dividing by two the computational cost.

$$\tilde{\overline{D}}_{ikl}\tilde{\varepsilon}^p_{kl} = \tilde{D}_{ikl}\tilde{\varepsilon}^p_{kl} + \tilde{D}_{ik+1l}\tilde{\varepsilon}^p_{k+1l} + i[\tilde{D}_{ik+1l}\tilde{\varepsilon}^p_{kl} - \tilde{\varepsilon}^p_{k+1l}\tilde{D}_{ikl}] \tag{35}$$

$$\begin{aligned} \overline{D}_{ikl} \otimes \overline{\varepsilon}^p_{kl} &= D_{ikl} \otimes \varepsilon^p_{kl} + D_{ik+1l} \otimes \varepsilon^p_{k+1l} \\ &+ i[D_{ik+1l} \otimes \varepsilon^p_{kl} - \varepsilon^p_{k+1l} \otimes D_{ikl}] \end{aligned} \tag{36}$$

This method is also applied to the stress field calculation from contact pressure σ^e. Complex influence coefficient is constructed as indicated in equation (37). Two terms of the stress tensor can then be calculated simultaneously, one given by the real part of the result, and the other one is given in the complex part.

$$\begin{aligned} &\overline{S}_{ijk} = S_{ijk} + iS_{i+1jk} \\ &\overline{p}_k = p_k \\ &\overline{S}_{ijk} \otimes \overline{p}_k = S_{ijk} \otimes p_k + iS_{i+1jk} \otimes p_k \end{aligned} \tag{37}$$

Residual stress field is calculated in the same way, by replacing p_k with ε_{kl}, S_{ijk} with C_{ijkl} and S_{i+1jk} with C_{i+1jkl}.

7 Results and Discussion

The aim of this section is to illustrate the ability of the model to deal with elastoplastic rough contact. Results presented in this paper correspond to the indentation of a rough elastoplastic half space by a smooth elastic sphere. Both have the same elastic properties:

E = 210000 MPa

$\nu = 0.3$

Roughness is modeled by a sinusoidal surface profile in the x direction, of wavelength 0.2 mm and amplitude 2 μm. Sixty points have been used along each surface axis (1.02 mm). The depth is meshed as deep as necessary. The contact half width is 0.51 mm and the corresponding Hertz pressure for two smooth surfaces is 2500 MPa.

The Swift law parameter is used to describe the plastic behavior of the material. Plastic strains are expressed in micro-deformation. The parameters describing the material are:

B = 1150 MPa

C = 4.0

n = 0.095

The load is applied from zero to the final load in 10 loading steps.

Figure 4 shows the area where plastic deformation occurs, in the (Oxz) plane, O being the center of the contact, and figure 5 shows this area in the plane z/a=0.066, just below the surface. One can see on these two figures that the plastically deformed area is as large as the contact zone, and that it is 0.3a deep, a being the semi width of the contact.

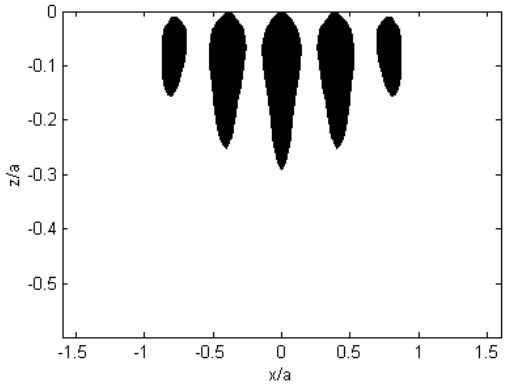

Figure 4 : Plastic zone in the plane y/a = 0.

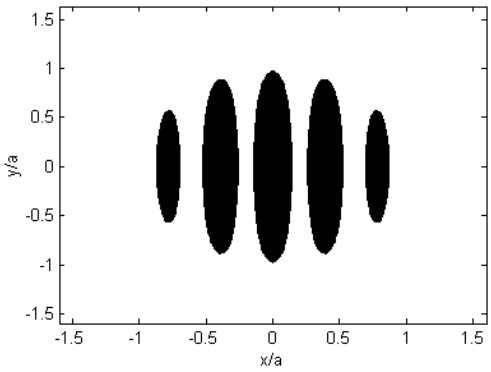

Figure 5 : Plastic zone in the plane z/a = 0.066.

Figure 6 shows the residual displacement induced by plastic strain. This is the displacement remaining after unloading (no plasticity occurs during unloading because of isotropic hardening). The profile shows that as summit of asperities are flattened, valleys move up thus reducing the amplitude of the roughness. However, the displacement remains very weak compared with the amplitude of roughness, as shown in figure 7. The pressure reduction is about the same magnitude.

Von Mises stress has been plotted along the z axis at the center of the contact (figure 8). The effect of the surface permanent deformation can be seen by comparing the elastic solution before (elastic contact curve) and after (pressure stress curve) plastic deformation. The pressure stress plot represents the Von Mises stress profile resulting from contact pressure, but does not integrate residual stresses. This effect can be compared with the effect of residual stress which can be more important, as seen in figure 8.

Last, the initial yield stress of the material is 0.311Ph, Ph

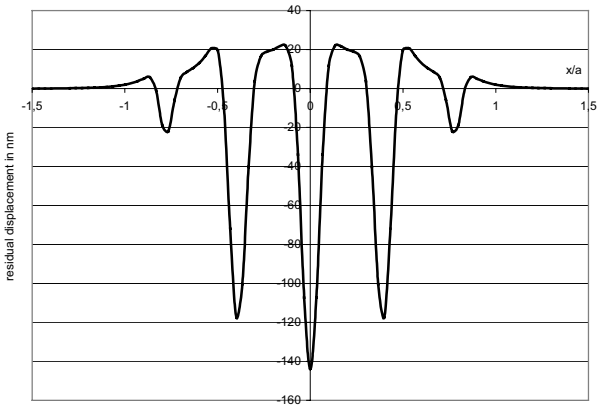

Figure 6 : Surface residual displacement due to plastic strain.

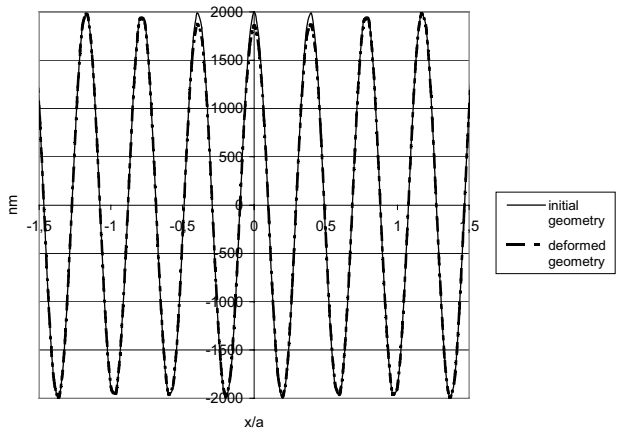

Figure 7 : Initial and plastically deformed roughness.

being the maximum hertzian pressure. Hence, one can see in figure 8 that the maximum hardened yield stress is 1.6 time higher than the initial one.

In this case, the main causes of elastic shakedown are the material behavior (hardening and residual stress) rather that the conformity of surfaces.

8 Conclusion

A full three dimensional numerical model of elastoplastic rough contact problem is presented. Based on a semi-analytical approach (half space assumption and boundary integral formulation), it allows one to discretize only the contact surface and the plastically deformed zone.

Furthermore, FFT are used to calculate all convolution products encountered in this problem. Special care has

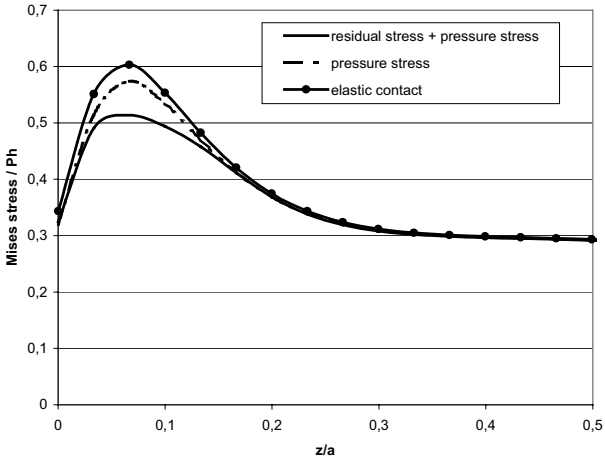

Figure 8 : Von Mises stress along the z axis at the center of the contact (normalized by the hertzian pressure Ph). Influence of surface conformity and of residual stresses.

been brought to minimize the number of points required to cancel the periodic effect due to the use of discrete Fourier transform. Last, complex influence coefficients and complex field values are used to minimize the number of FFT and IFFT required to perform convolution products. The use of FFT drastically reduces the computational cost enabling then the study of rough contact where a large number of points is required.

The resulting values supplied by the elastoplastic contact code of residual stresses, accurate stresses due to contact pressure, and hardening of the material are essential to the rolling fatigue contact analysis.

In this study, the whole problem is divided into an elastic part, which corresponds to a classical elastic contact problem, and a residual part, which accounts for plastic flow in bulk. The originality of this work lies in the treatment of the residual problem. The elastic part is considered as a normal, dry, frictionless contact.

Therefore, the residual part can be coupled with a more complex elastic problem as, for example, elastohydrodynamic or dry frictional contacts.

References

Archard, J.F.; Hunt, R.T.; Onions, R.A. (1975): Stylus Profilometry and the Analysis of the Contact of Rough Surfaces, *The Mechanics of the Contact Between Deformable Bodies*, Delft University Press, pp. 282-303.

Bailey, D.M.; Sayles, R.S. (1991): Effect of Roughness

and Sliding Friction on Contact Stresses, *ASME Journal of Tribology*, Vol. 113, pp. 729-738.

Barber, J.R.; Ciavarella, M. (2000): Contact Mechanics, *Int. J. Solids Struct.*, Vol. **37**, pp. 29-43.

Brebbia, C.A.; Telles, J.F.C.; Wrobel, L.C. (1984): *Boundary Element Techniques*, Springer-Verlag, Berlin, 466 p.

Brigham, E.O. (1974): *The Fast Fourier Transform*, Prentice-Hall, Englewood Cliffs, 252 p.

Chiu, Y.P. (1977): On the Stress Field Due to Initial Strains in a Cuboid Surrounded by an Infinite Elastic Space, *ASME Journal of Applied Mechanics*, pp. 587-590.

Chiu, Y.P. (1978): On the Stress Field and Surface Deformation in a Half Space With a Cuboidal Zone in Which Initial Strains Are Uniform, *ASME Journal of Applied Mechanics*, pp. 302-306.

Greenwood, J.A.; Williamson, J.B.P. (1966): Contact of Nominally Flat Surfaces, *Proc. Roy. Soc.*, London, Vol. 295, pp. 300-319.

Jacq, C.; Nélias, D.; Lormand, G.; Girodin, D. (2002): Development of a Three-Dimensional Semi-Analytical Elastic-Plastic Contact Code, *ASME Journal of Tribology* (in press).

Johnson, K.L. (1985): *Contact Mechanics*, Cambridge University Press, Cambridge, 417 p.

Kalker, J.J. (1990): *Three-Dimensional Elastic Bodies in Rolling Contact*, Kluwer Academic Publishers, Dordrecht, 314 p.

Komvopoulos, K.; Choi, D.H. (1992): Elastic Finite Element Analysis of Multi-Asperity Contacts, *ASME Journal of Tribology*, Vol. 114, pp. 823-831.

Liu, G.; Wang, Q.; Liu, S. (2001): A Three-Dimensional Thermal-Mechanical Asperity Contact Model for Two Nominally Flat Surfaces in Contact, *ASME Journal of Tribology*, Vol. 123, pp. 595-602.

Liu, G.; Wang, Q.; Liu, S. (2000): A Versatile Method of Discrete Convolution and FFT (DC-FFT) for Contact Analyses, *Wear*, Vol. 243, pp. 101-111.

Lubrecht, A.A.; Ioannides, S. (1991): A Fast Solution of the Dry Contact Problem and the Associated Sub-Surface Stress Field, Using Multilevel Techniques, *ASME Journal of Tribology*, Vol. 113, pp. 128-133.

Mayeur, C.; Sainsot, P.; Flamand, L. (1995), A Numerical Elastoplastic Model for Rough Contact, *ASME Journal of Tribology*, Vol. 117, pp. 422-429.

Nogi, T.; Kato, T. (1997): Influence of a Hard Surface Layer on the Limit of Elastic Contact - Part I: Analysis Using a Real Surface Model, *ASME Journal of Tribology*, Vol. 119, pp. 493-500.

Polonsky, I.A.; Keer, L.M. (2000a): A Fast and Accurate Method for Numerical Analysis of Elastic Layered Contacts, *ASME Journal of Tribology*, Vol. 122, pp. 30-35.

Polonsky, I.A.; Keer, L.M. (2000b): Fast Methods for Solving Rough Contact Problems: A Comparative Study, *ASME Journal of Tribology*, Vol. 122, pp. 36-41.

Seabra, J.; Berthe, D. (1987): Influence of Surface Waviness and Roughness on the Normal Pressure Distribution in the Hertzian Contact, *ASME Journal of Tribology*, Vol. 109, pp. 462-470.

Telles, J.F.C.; Brebbia, C.A. (1981): New Developments in Elastoplastic Analysis, *Boundary Element Methods*, Springer-Verlag, pp. 350-370.

Tichy, J.A.; Meyer, D.M. (2000): Review of Solid Mechanics in Tribology, *Int. J. Solids Struct.*, Vol. 37, pp. 391-400.

Webster, M.N.; Sayles, R.S. (1986): A Numerical Model for the Elastic Frictionless Contact of Real Rough Surfaces, *ASME Journal of Tribology*, Vol. 108, pp. 314-320.

Zhao, Y.W.; Maietta, D.M.; Chang, L. (2000): An Asperity Microcontact Model Incorporating the Transition from Elastic Deformation to Fully Plastic Flow, *ASME Journal of Tribology*, Vol. 122, pp. 86-93.